Surfaces and Interfaces 62 (2025) 106207

Contents lists available at ScienceDirect

Surfaces and Interfaces

journal homepage: www.sciencedirect.com/journal/surfaces-and-interfaces

Glucosyl OPE-modified halloysite nanotubes and their potential as phototherapy agents for bacterial infections

Aurora Mancuso [a,1], Marina Massaro [b,1], Federica Leone [b], Paola Maria Bonaccorsi [a], Giuseppe Compagnini [c], Chiara Maria Antonietta Gangemi [a], Fausto Puntoriero [a], Maria Ribagorda [d], Vittorio Scardaci [c], César Viseras [e,f], Serena Riela [c,*], Anna Barattucci [a,*]

[a] Dipartimento di Scienze Chimiche, Biologiche, Farmaceutiche ed Ambientali (CHIBIOFARAM), Università di Messina, Viale F. Stagno d'Alcontres, 31, 98166, Messina, Italy
[b] Dipartimento di Scienze e Tecnologie Biologiche, Chimiche e Farmaceutiche (STEBICEF), Università di Palermo, Viale delle Scienze, Parco d'Orleans II, Ed. 17, 90128 Palermo, Italy
[c] Dipartimento di Scienze Chimiche (DSC), Università di Catania, Viale Andrea Doria 6, 95125, Catania, Italy
[d] Departamento de Química Orgánica, Institute for Advanced Research in Chemical Sciences (IAdChem), Ciudad Universitaria de Cantoblanco, C. Francisco Tomás y Valiente, 7, Fuencarral-El Pardo, 28049 Madrid, Spain
[e] Department of Pharmacy and Pharmaceutical Technology, Faculty of Pharmacy, University of Granada, Campus Universitario de Cartuja, 18071 Granada, Spain
[f] Andalusian Institute of Earth Sciences, CSIC-UGR, 18100 Armilla, Granada, Spain

ARTICLE INFO

Keywords:
Oligo(phenylene ethynylene)
Halloysite
Covalent modification
Photodynamic therapy
Antibiotics

ABSTRACT

Bacterial infections pose a significant health threat, worsened by the growing issue of antibiotic resistance and biofilm formation. Phototherapies, particularly photodynamic therapy (PDT), offer promising non-invasive alternatives due to their high efficacy and minimal side effects. These therapies utilize photosensitizers (PSs), which, when activated by light, generate reactive oxygen species (ROS) that lead to bacterial cell death. Recent advancements have focused on enhancing PDT by integrating PSs with nanomaterials. Halloysite nanotubes (HNTs), a natural clay mineral, are of particular interest due to their unique properties, including intrinsic antibacterial activity and the ability to integrate into bacterial biofilms. By combining HNTs with photosensitizers, we aimed to improve treatment efficacy. In this study, we synthesized a novel glucosyl OPE derivative and covalently attached it to HNTs, forming the composite **HNTs@Glu-OPE**. This system was thoroughly characterized, and its ROS generation capabilities were tested under 365 nm light irradiation using uric acid as a probe. Loaded with vancomycin, **HNTs@Glu-OPE** represents a multifunctional approach to PDT, enhancing both the delivery and effectiveness of therapeutic agents against resistant bacterial strains.

1. Introduction

Bacterial infections are among the most common causes of human death. The infections caused by *Staphylococcus aureus* account for approximately 50% of clinical infections. Antibiotic treatment is the standard approach for bacterial infections, that are often accompanied by biofilm formation. Furthermore, antibiotic resistance remains a significant challenge, highlighting the need for new methodologies to address these diseases [1,2].

In recent years, phototherapies, including antibacterial photodynamic therapy (aPDT) [3] and photothermal therapy (PTT) [4], have gained attention for their non-invasive nature, ease of operation, high therapeutic efficacy, and minimal side effects compared to conventional therapies. These therapies function through photosensitizers (PSs) [5], or photothermal agents [6], and light at appropriate wavelengths to generate, in the case of aPDT, reactive oxygen species (ROS), especially $^1O_2$, which cause oxidative damage to the cellular components, and in the case of PTT, hyperthermia, leading to cell growth arrest or cell death. Various chemical compounds have been investigated as PSs, including boron dipyrromethene (Bodipy) derivatives [7],

* Corresponding authors.
E-mail addresses: serena.riela@unipa.it (S. Riela), anna.barattuci@unime.it (A. Barattucci).
[1] These authors equally contributed to the work.

https://doi.org/10.1016/j.surfin.2025.106207
Received 21 October 2024; Received in revised form 5 February 2025; Accepted 10 March 2025
Available online 11 March 2025

transition metal complexes [8], porphyrins [9], cyanines [10]. However, the current performance of PSs remains unsatisfactory due to issues such as low water solubility, aggregation in aqueous solutions, limited photostability, and rapid photobleaching. Thus, developing suitable PSs is essential for the broader application of PDT [11].

Recent studies have demonstrated that combining versatile nanomaterials with PSs can enhance both the efficacy of the PSs and the therapeutic outcomes of PDT [12]. Nanomaterials such as liposomes or polymeric nanostructures can act as PS carrier, improving properties like hydrophilicity, photochemical stability, local accumulation, and overall biocompatibility. In contrast, nanomaterials like mesoporous silica or graphene-based nanotubes can synergistically enhance ROS production and facilitate deeper cellular penetration [13]. Furthermore, the ease of functionalization and the large surface area of certain nanomaterials allow for the integration of PDT with targeted therapies, such as the incorporation of specific drugs, leading to the development of promising multi-agent platforms for treating specific diseases [14].

Among the different nanomaterials for these purposes, especially when aPDT is considered, clay minerals are particularly valuable candidates. Clay minerals have long been recognized for their healing properties, largely due to their intrinsic antibacterial activity, which varies depending on their structure and composition [15,16]. Halloysite, a natural aluminosilicate clay from the kaolin group, interacts with cells through electrostatic attraction, hydrophobic interactions, and van der Waals forces. It effectively interacts with bacterial cells, which secrete a biopolymeric matrix that incorporates the clay into their biofilms [17]. Morphologically, halloysite naturally occurs as halloysite nanotubes (HNTs), with aluminol groups exposed on the lumen and siloxane groups on the external surface [18]. Although HNTs themselves do not possess antibacterial activity, selectively modifying their surfaces [19–21], either covalently or supramolecularly, paves the way for creating promising nanomaterials with enhanced biological activities for combating common pathogens [22,23].

Oligo(phenylene ethynylene)s (OPEs), luminescent linear oligomers with extended conjugated aromatic and ethynylenic moieties, have gained significant research interest due to their synthetic versatility, notable photophysical and photochemical properties, tunable electronic structures, notable bioactivity, and ability to generate singlet oxygen [24]. Monnereau and Andraud [25], first demonstrated that the presence of bromine on the aromatic rings improved the singlet oxygen production yield, suggesting OPEs as potential PSs for PDT. In the same year, Whitten and Schanze [26] reported using cationic end-only functionalized OPEs to prevent and eliminate *Escherichia coli* (E. *coli*) biofilms. This water-soluble family of conjugated oligomers showed affinity for bacterial cell membranes and exhibited light-activated biocidal activity, causing membrane disruption, agglomeration, and death of both Gram-positive and Gram-negative bacteria. The capability of OPEs to penetrate the bacterial membrane and produce ROS species has paved the way for their use as PSs in aPDT [27]. Additionally, OPEs have been shown to selectively bind to the aggregate conformations of certain amyloid proteins, suggesting their potential as PSs for treating diseases such as Alzheimer's disorder [28].

Previously, we prepared highly luminescent and biocompatible OPE derivatives with one or two NMe_2 groups on the aromatic OPE residue and two glucose terminations. It was demonstrated that the lone electron pair on the nitrogen atom of the NMe_2 group was crucial for these OPEs to produce ROS and be used in superficial PDT [29]. Excited by UVA light, the synthesized OPEs exerted a significant photodynamic effect, triggering mitotic blockage and causing tumoral cell death even with low oxygen production [30]. Further studies on mannose- and maltose-decorated OPEs highlighted Golgi or lysosome internalization, depending on the sugar moieties, and a good photodynamic effect under irradiation at 450 nm for blue light-induced PDT [31].

Herein, we report the design and synthesis of a new glucosyl OPE derivative (**Glu-OPE**) and its covalent grafting onto the external surface of HNTs (**HNTs@Glu-OPE**). This nanomaterial was thoroughly characterized, and its capability to produce ROS species useful for PDT was evaluated chemically by monitoring changes in the UV–*vis* spectra of uric acid, chosen as chemical probe under LED irradiation. Additionally, to develop functional nanomaterials for treating bacterial infections, the **HNTs@Glu-OPE** nanomaterial was loaded with vancomycin as an antibiotic model. Finally, kinetic release experiments were performed in media mimicking physiological conditions. This synthetic approach aimed to develop a multifunctional nanosystem with PS characteristics for PDT by combining the features of OPEs with those of HNTs. Moreover, the formation of a glycosidic shell around the system could enhance biocompatibility to the decorated nanoparticles and selectivity for sugar-avid cancer cells [32], potentially leading to effective treatments for severe antibacterial infections.

2. Results and discussion

2.1. Synthesis of OPE Glu-OPE

The most significant synthetic steps to obtain **Glu-OPE** are outlined in Scheme 1. **Glu-OPE** was obtained starting from commercially available products, in a divergent approach for the desymmetrisation of the OPE aromatic chain. The complete synthesis of **Glu-OPE** is described in Supporting Information (SI). The cross-coupling of 2-propynyl-O-β-glucopyranoside-2,3,4,6-tetraacetate [33] and commercially available 1, 4-diiodo-2,5-dimethoxy benzene [34], in a 1:2 ratio, was the first of several other couplings, performed to link the bricks of OPE, in the presence of catalytic amount of $Pd(PPh_3)_4$ or $Pd(PPh_3)_2Cl_2$ or using copper-free Sonogashira conditions, necessary when TMS function was introduced into the chain. The acetylated glucose termination and the trimethylsilyl group were simultaneously deprotected with K_2CO_3.

A copper(II)-catalyzed azide alkyne cycloaddition (CuAAC), in a mixture 1:1 of DMF and water, between the deprotected OPE and 5-Azido-valeric acid [35], was the last step performed to afford the "diverse-ended" **Glu-OPE. Glu-OPE** was extracted with ethyl acetate from the aqueous solution of the click reaction and washed several times with ethyl ether to obtain a bright orange powder that was fully characterized by NMR experiments.

2.2. Synthesis of halloysite-based OPE (HNTs@Glu-OPE)

Amino modified HNTs were used as scaffold (HNTs-NH_2) for the synthesis of the halloysite-based OPE (**HNTs@Glu-OPE**). The covalent grafting of **Glu-OPE** on HNTs-NH_2 was performed at room temperature for 48 h, in the presence of 1-ethyl-3-(3-dimethylaminopropyl)carbodiimide) (EDC) as shown in Scheme 2. The obtained **HNTs@Glu-OPE** nanomaterial was isolated as a yellow pale powder after washings of the crude product with H_2O, MeOH and DCM to remove both the catalyst and residual unreacted reagents. Based on the stoichiometric ratios between HNTs-NH_2 and **HNTs@Glu-OPE** (0.63 mmol g^{-1} and 0.01 mmol g^{-1}, respectively), it was found that complete linkage of **Glu-OPE** on the HNTs surface is not achieved. This finding is probably due to steric hindrance and could be beneficial to improve the cellular uptake due to the presence of some free amino groups [36]. These indeed, being protonated into physiological conditions could establish favourable interactions within cellular membranes.

The **HNTs@Glu-OPE** nanomaterial was characterized by FT-IR spectroscopy and TGA, and the colloidal properties were estimated by DLS and ζ-potential measurements. Furthermore, the morphology of the nanomaterial was imaged by TEM and high-angle annular dark field scanning transmission electron microscopy (HAADF-STEM). Fig. 1A shows the FT-IR spectra of **HNTs@Glu-OPE** and HNTs-NH_2 nanomaterials. The assignments for the bands of HNTs-NH_2 can be done based on literature data [37]. The FT-IR spectrum of **HNTs@Glu-OPE** exhibits all the band attributable to the inorganic nanomaterial and the bands due to the organic portion at ca. 3450 cm^{-1} corresponding to the stretching of the hydroxyl groups, and the bands in the range 1420–1310

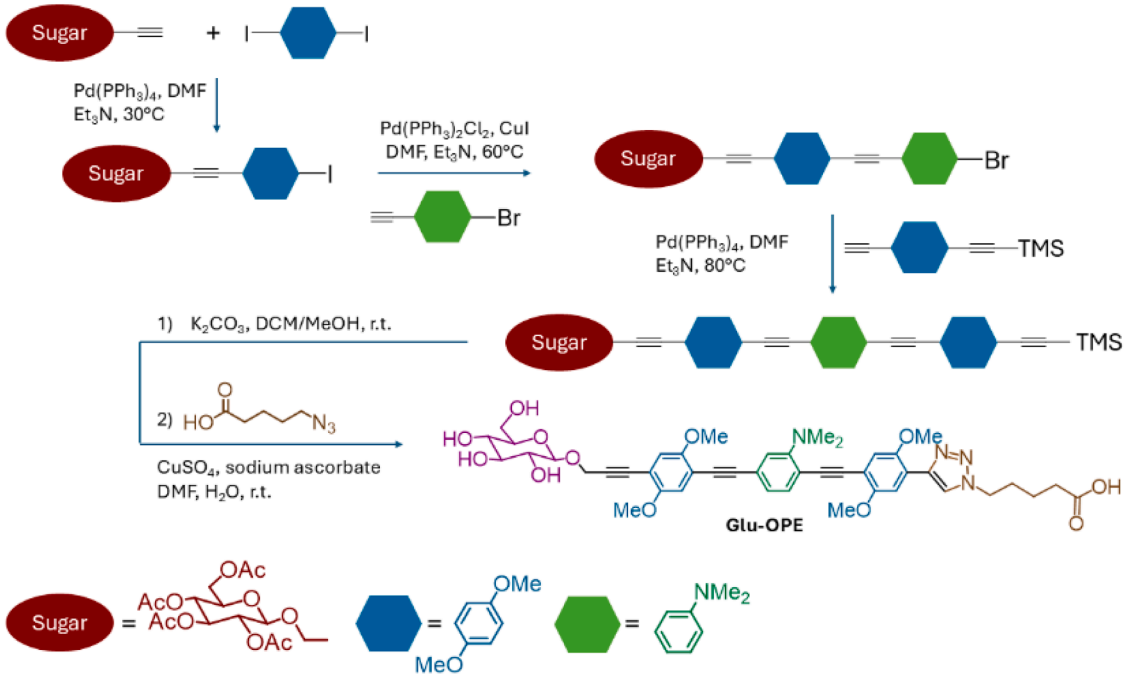

Scheme 1. Schematic synthesis of **Glu-OPE**.

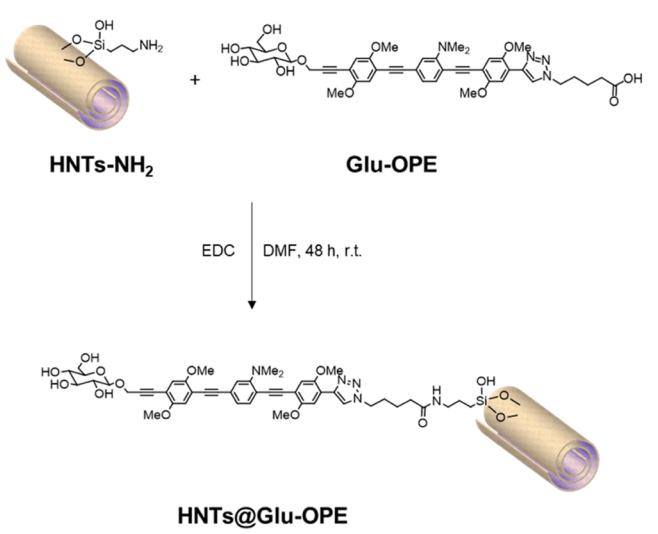

Scheme 2. Schematic representation of the synthesis of **HNTs@Glu-OPE** nanomaterial.

cm^{-1}, arising from stretching vibrations of C=N and N=N of triazole groups.

Fig. 1B shows the TGA curves of the HNTs-NH_2 and **HNTs@Glu-OPE** nanomaterials for comparison. Beside the typical mass losses of halloysite, arising from the expulsion of the interlayer water molecules of HNTs (ca. 550 °C) and that due to the degradation and volatilization of organic matter in HNTs-NH_2 (ca. 250 °C), a further degradation step in the TGA curve of **HNTs@Glu-OPE** can be appreciated. The amount of **Glu-OPE** grafted onto HNTs surface was calculated by considering the residual masses at 800 °C. DLS measurements allow the determination of the structural characteristics of the nanomaterials by monitoring their mobility in water and by measuring the average translational diffusion coefficient. This coefficient considers the dimension, shape, and hydration of the diffusing particles and, further, the existence of aggregation phenomena. By applying the Stokes–Einstein equation it is possible to calculate the average diameter of the equivalent sphere, which can be considered as an index to follow the changes in particle dimensions and interparticle aggregation. The **HNTs@Glu-OPE** nanomaterial showed a Z-average size very large (>1000 nm) with a high polydispersity index as large as ca. 0.69 (Fig. 1D). Since the polydispersity index (PI) is a measure of the heterogeneity of a sample based on size, it is possible to conclude that in our case we observe a broad size distribution of diffusing objects. The modification of halloysite external surface was also verified by ζ-potential measurements, that showed that **HNTs@Glu-OPE** possesses a ζ-potential value of -6.90 mV, more positive than pristine HNTs (- 20 mV).

The above findings were also confirmed by turbidimetric analyses (Fig. 1C) that showed that introduction of compound **Glu-OPE** onto HNTs external surface affected the aqueous stability of **HNTs@Glu-OPE** compared to the HNTs-NH_2 nanomaterial.

The morphology of the nanomaterial was imaged by TEM and high-angle annular dark field scanning transmission electron microscopy (HAADF-STEM). In comparison to the HNTs-NH_2 precursor (Fig. 2A), the **HNTs@Glu-OPE** nanomaterial (Fig. 2B-C) exhibits the characteristic hollow tubular structure of halloysite but organized in compact clusters probably due to the presence of the organic molecules onto the external surface which could establish favourable interactions such as π−π interactions. From elemental mapping extrapolated by energy-dispersive X-ray spectroscopy EDS measurements it is possible to observe that in **HNTs@Glu-OPE**, the organic molecules are uniformly distributed onto the HNTs external surface, as showed by the mapping of C atoms. EDS measurements (Fig. 2G) on a selected area also show the presence of C atoms, beside the typical elements of halloysite, corroborating the successful synthesis.

2.3. *Photophysical studies of Glu-OPE*

The photophysical properties of OPE **15**, taken as reference compound (see ESI), and **Glu-OPE** are presented in Fig. 3. Both species exhibit absorption spectra in water characterized by intense and broad bands (λ: 367 nm - ε in DCM: 38,500 M^{-1} cm^{-1}), primarily due to π-π* transitions. In DCM, an additional lower energy feature is observed (appearing as a shoulder at 410 nm), which can be attributed to partial

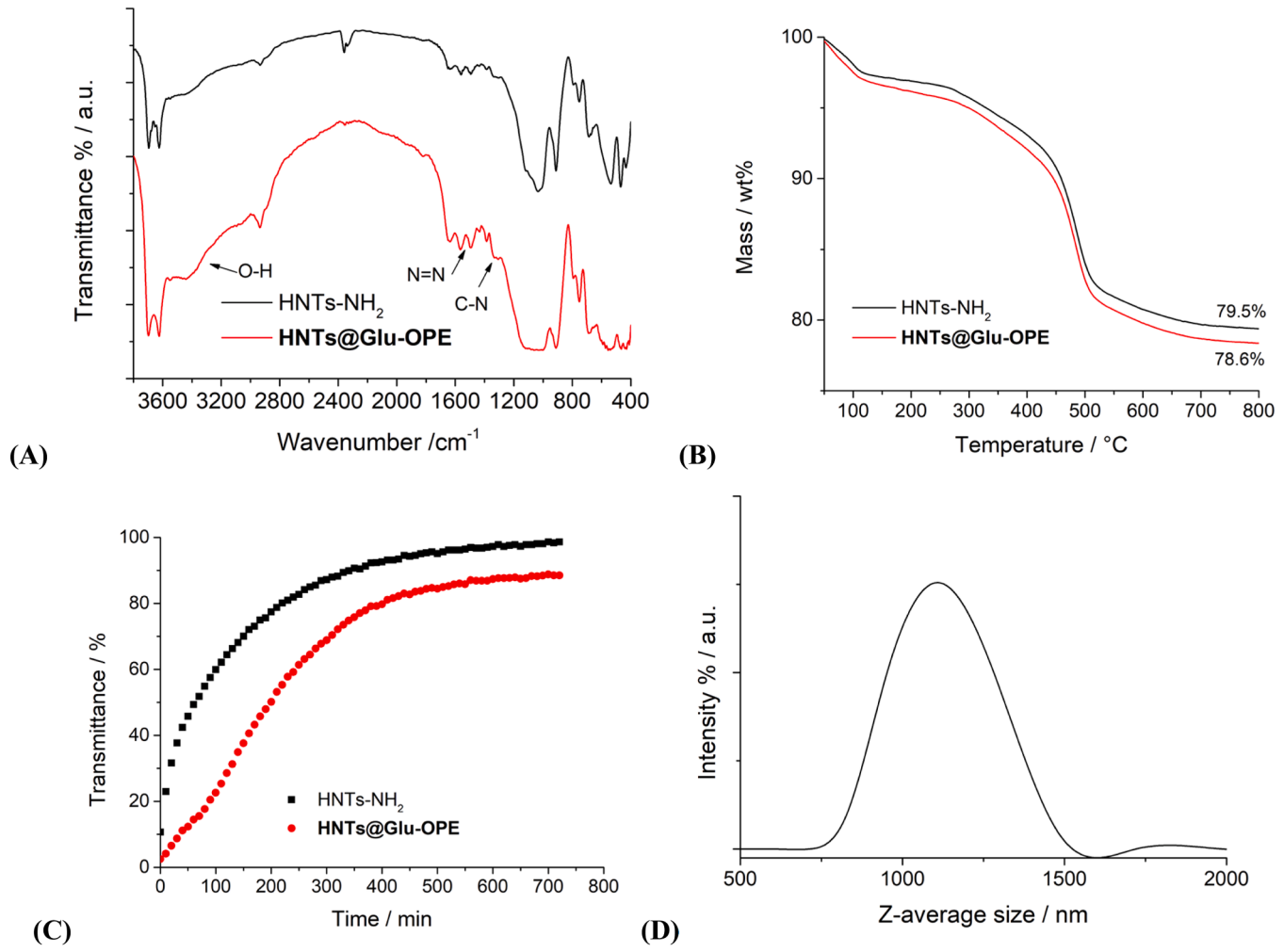

Fig. 1. (A) FT-IR spectra and (B) thermoanalytical curves of HNTs-NH_2 and **HNTs@Glu-OPE** nanomaterials and (C) turbidimetric analysis of aqueous dispersion of HNTs-NH_2 and **HNTs@Glu-OPE** (1 mg mL^{-1}) nanomaterials; (D) Distribution functions of the Z-average size value of **HNTs@Glu-OPE** nanomaterial.

charge-transfer interactions facilitated by the amine group.

At room temperature, both OPEs display luminescence in aqueous solution and in DCM. Notably, the emission spectra in water are red-shifted and exhibit, independently of the excitation wavelength, a broader profile compared to those in DCM, indicating that water more effectively stabilizes the charge-transfer state. In DCM the luminescence quantum yield of **15** and **Glu-OPE** is about 50% while in water decreases to 20% (see Table S1 for more details). The similarity in both absorption and emission spectra between the two species indicates that their photophysical properties are primarily governed by the central conjugated chain, with the triazole ring having negligible impact.

2.4. Photophysical studies of HNTs@Glu-OPE

The UV–*vis* spectrum of a **HNTs@Glu-OPE** dispersion (1 mg mL^{-1}) in MeOH showed intense broad low-energy absorption bands centered at ca. 370 nm (Fig. 4). Similar to compound **Glu-OPE**, this absorption in the UV region could be due to spin-allowed $\pi-\pi^*$ transitions and is attributed to Internal Change Transfer (ICT) transitions. The excitation of **HNTs@Glu-OPE** allowed the appearance of an emission band in the blue region of the spectrum, centered at ca. 470 nm with a shoulder at 520 nm (Fig. 4).

The shape of the spectrum obtained under these experimental conditions, which is more structured than the solution, suggests a lower degree of mobility of the OPE on the structure of the HNTs.

To verify if the synthetized **HNTs@Glu-OPE** possesses any photosensitizer properties, preliminary studies were performed by observing the ROS production capacity by UV–*vis* spectroscopy. In particular, the UV–*vis* spectrum changes of uric acid (UA), a typical ROS scavenger, were monitored [30,38]. As shown in Fig. 5, the UV–*vis* absorbance intensity of UA in the presence of **HNTs@Glu-OPE** nanomaterial (1 mg mL^{-1}) decreased under the laser irradiation indicating that the nanomaterial could exert some effects. Conversely, the UV–*vis* absorption of the UA solution did not show any change in the absorbance under laser irradiation in absence of the **HNTs@Glu-OPE** nanomaterial or in the presence of pristine HNTs (Figure S13).

The quantum yield of ROS production (Φ_{ROS}) was calculated to be 0.23, higher than that of **15** (Φ_{ROS} = 0.15)[31] indicating that the combination of **Glu-OPE** with halloysite gives rise to a nanomaterial with improved properties.

2.5. Loading of vancomycin into HNTs@Glu-OPE lumen

Previous studies demonstrated that halloysite shows no cytotoxicity on normal human dermal fibroblasts within 24 h [23] and the **Glu-OPE** is not toxic on different cell lines [30,31], so the developed nanomaterial could be a valuable biocompatible candidate for future antibacterial applications. In light of these premises, to develop multifunctional materials to treat severe bacterial infections, the **HNTs@Glu-OPE** nanomaterial was loaded with an antibacterial specie as vancomycin. The combination of PDT and the drug could be crucial as tools to manage and inactivate superficial bacterial infections accessible to light [39].

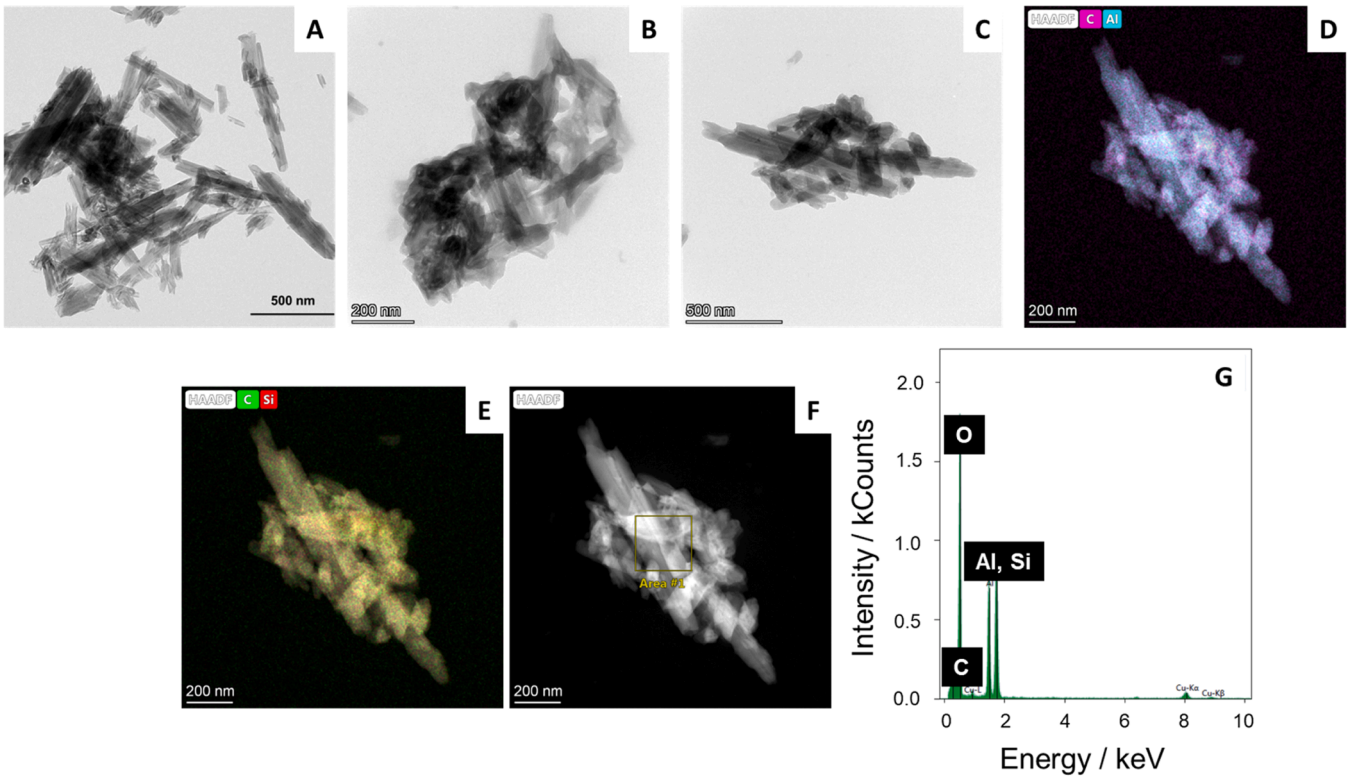

Fig. 2. (A-C) TEM images of (A) HNTs-NH_2 nanomaterial and (B-C) **HNTs@Glu-OPE**; (D-F) HAADF/STEM of the **HNTs@Glu-OPE** nanomaterial with elemental mapping images; (G) EDS analysis on the selected area.

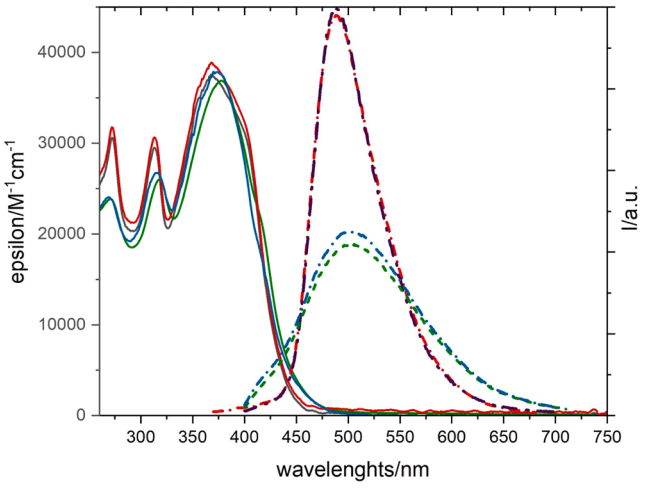

Fig. 3. Absorption (full line) and emission spectra (dotted and dashed lines) of **15** (blue in water and red in DCM) and **Glu-OPE** (green in water and black in DCM) at room temperature.

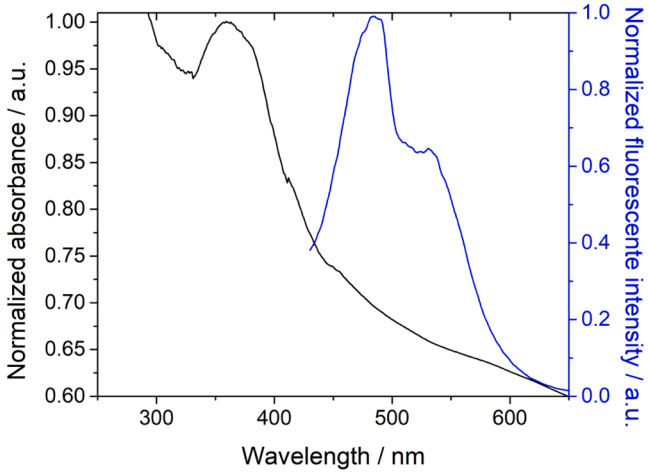

Fig. 4. Absorption (black line) and emission (blue line) spectra of **HNTs@Glu-OPE** nanomaterial (1 mg mL^{-1}, 25 °C) in MeOH.

Using a common strategy for loading active species inside HNTs carriers [20], vancomycin was loaded onto the **HNTs@Glu-OPE** nanomaterial. In details, a dispersion of halloysite (5 mL, acetone) was mixed with a concentrated vancomycin solution (H_2O; 10^{-2} M, 1 mL). Afterward, the dispersion was evacuated for 3−5 min to promote the loading of the molecule into the lumen and left to stir at room temperature for 18 h.

After work-up, the nanomaterial (**HNTs@Glu-OPE**/Van) showed a drug loading of ca. 16 wt% with an entrapment efficiency of ca. 94%, as highlighted by UV–*vis* measurements. The successful loading was verified by FT-IR spectroscopy (see SI), which confirm the loading of the drug on the **HNTs@Glu-OPE** nanomaterial. Thus, kinetic release experiments of vancomycin from **HNTs@Glu-OPE**/Van were performed was evaluated by the dialysis bag method at pH 7.4 and pH 5.5, the latter to mimic skin's pH for potential topical treatment.

The obtained kinetic data are reported in Fig. 6. The release of vancomycin from **HNTs@Glu-OPE**/Van was very fast at pH 5.5 where the total amount of drug loaded was released after ca. 300 min. Conversely, in neutral conditions, the drug is fast released in the first 200 min, reaching the total amount released after 24 h. This different behaviour could be ascribed to the fact that at pH 5.5, below the isoelectric point of HNTs (pH ca. 6.5) [40], the tubes are in their zwitterionic form, whereby electrostatic repulsions with the positively charged drugs could exist, fasting the release.

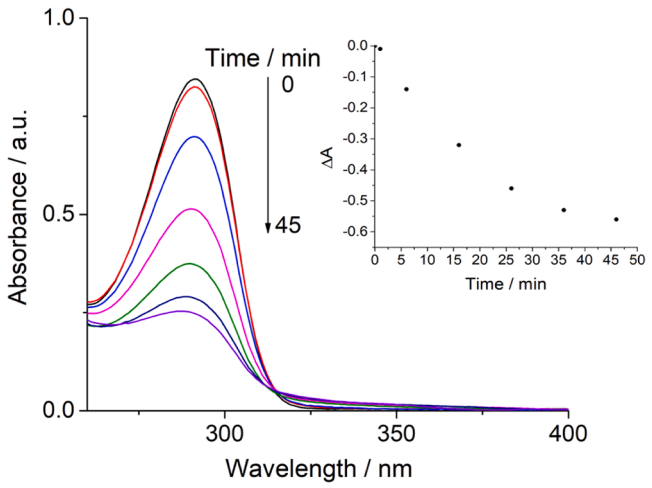

Fig. 5. Degradation of uric acid (λ_{max} = 290 nm) as a function of time in the presence of **HNTs@Glu-OPE** (1 mg mL^{-1}, corresponding to [**Glu-OPE**] = 14 μM), irradiated at 365 nm.

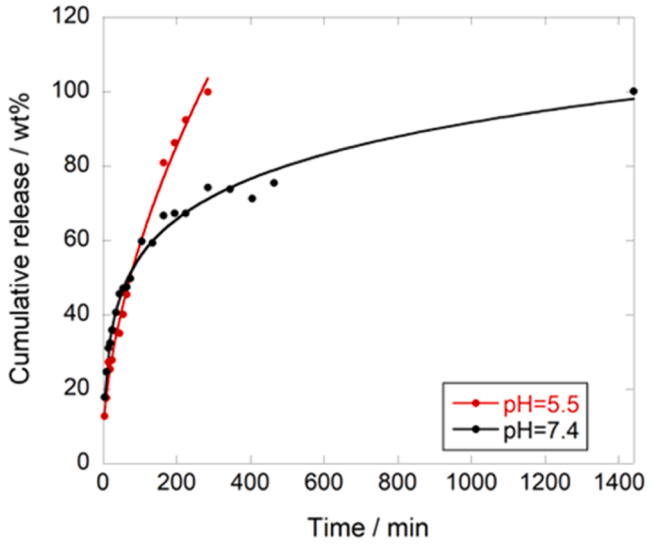

Fig. 6. Kinetic release of vancomycin from **HNTs@Glu-OPE**/Van in phosphate buffer (50 mM) at pH 5.5 and 7.4, at 37 °C.

Many bacterial infections, particularly those caused by *Staphylococcus aureus* are associated with microenvironment characterized by acidic pH [41]. Thus, the fast release in acidic medium of vancomycin enhances its effectiveness by ensuring an optimal drug concentration for inhibition of bacteria growth.

The kinetic data were analysed by different mathematical models to assess the release mode of vancomycin from the carrier. It was found that at both pH, the kinetic data follow a Power fit model, indicating that the release is ruled by a Fickian mechanism (k = 127 ± 71 min^{-1}, n = 0.08 ± 0.03, R^2 = 0.98762 and $k = 4.1 \pm 1.7$ min^{-1}, $n = 0.56 \pm 0.006$, R^2 = 0.99218, for pH 7.4 and pH 5.5, respectively).

3. Experimental section

3.1. Synthesis

Glu-OPE. 5-azidopentanoic acid **16** (0.04 g, 0.26 mmol, 1.2 eq.) was added to a solution of **15** (see SI) (0.15 g, 0.22 mmol, 1 eq.), sodium ascorbate (5 mg, 0.02 mmol, 0.1 eq.), and copper sulphate (0.08 g, 0.52 mmol, 2 eq.) in a mixture of DMF (9 mL) and water (1 mL) at room temperature. The reaction mixture was maintained under continuous stirring at room temperature for 1 h, until the disappearance of the starting compound **15** by TLC (acetonitrile/DCM 70:30). The reaction was extracted with ethyl acetate (3 × 15 mL) and the combined organic layers were washed with brine (3 × 15 mL), dried over anhydrous Na_2SO_4, filtered, and concentrated *in vacuum*. **Glu-OPE** was obtained as a yellow solid and underwent further purification with ethyl ether to afford a bright orange powder (0.13 g, 0.16 mmol, 75%).

TLC: *Rf* =0.25 (acetonitrile/DCM 70:30). Mp=147–149°C. ^{1}H NMR (dmso-*d6*): δ 8.46 (s,1H, H-t), 7.82 (s, 1H, H-6), 7.46 (d, $J_{5',6'}$= 8.3, 1H, H-6′), 7.20, 7.18 and 7.09 (three s, 3H, H-3, 3″, 6″), 7.03 (m, 2H, H-3′, 5′), 5.16 (bd, 1H, OH), 5.03 (bs, 1H, OH), 4.97 (bd, 1H, OH), 4.68 and 4.55 (m AB system, J_{gem} = 15.7, 3H, $CH_2C\equiv$ and 6″-OH), 4.42 (bt, 2H, CH_2N), 4.34 (d, $J_{1'',2''}$ =7.9, 1H, H-1″), 3.92, 3.90, 3.83 and 3.82 (four s, 12H, 4 x OCH_3), 3.71–3.03 (m, 5H, H-2″, 6″), 3.32 (2H, CH_2CO), 3.00 [s, 6H, $N(CH_3)_2$], 1.87 (bt, 2H, CH_2CH_2N), 1.45 (bs, 2H, CH_2CH_2CO). ^{13}C NMR (dmso-*d6*): δ 208.2, 155.0, 154.9, 154.8, 150.1, 142.3, 135.6, 126.2, 125.0, 124.8, 121.3, 119.9, 117.5, 117.4, 116.3, 114.6, 114.5, 113.2, 110.5, 102.3, 96.0, 94.8, 92.5, 88.1, 83.5, 80.0, 79.8, 78.0, 77.8, 74.3, 70.8, 61.5, 57.1, 57.0, 56.1, 44.2, 31.4. Anal. Calcd for $C_{44}H_{48}N_4O_{12}$ (824.88): C, 64.07; H, 5.87; N 6.79. Found: C, 63.98; H, 5.88; N 6.81.

3.2. Synthesis of HNTs@Glu-OPE

Glu-OPE (5.0 mg, 6.1 × 10^{-3} mmol) was suspended in DMF (10 mL), and 1- Ethyl-3-(3′-dimethylaminopropyl)carbodiimide (EDC, HCl) (1.2 mg, 6.1 × 10^{-3} mmol) was added. The suspension was stirred under an argon atmosphere at room temperature for 10 min. Then, HNTs-NH_2 (100 mg) was quickly added. The mixture was stirred for 48h. Then, the solvent was removed by filtration; the powder was then rinsed successively with H_2O, MeOH and DCM and finally dried at 80 °C under vacuum.

3.3. Single oxygen generation

The generation of ROS was evaluated by using uric acid (UA) as ROS scavenger under the UVA light (365 nm) irradiation. To an aqueous solution of UA (50 μM, 2 mL), 2.4 mg of **HNTs@Glu-OPE** were added. The obtained dispersion was transferred to a quartz cuvette with four faces of 1.00 cm of optical length and then stirred under LED irradiation at wavelength of 365 nm (740 mW). At predetermined time, the dispersion was centrifuged, and the supernatant solution was analyzed by UV–*vis* spectroscopy. LEDs were sourced from Prizmatix.

The quantum yield of ROS production was evaluated by monitoring the degradation profile of uric acid over time, irradiating a suspension of **HNTs@Glu-OPE** (*x*) in the presence of uric acid using a laser at 365 nm (740 mW and photon flux of 1.86 × 10^{-6} einstein/s), and comparing it to the degradation profile in the presence of a standard (*r*), methylene blue (reference - quantum yield of ROS production: 0.5) by irradiating with a laser at 650 nm (200 mW and photon flux of 7.95 × 10^{-7} einstein/s).

The number of photons absorbed per unit of time was calculated by considering the portion of photons absorbed by the samples, based on the transmittance (*T*) value under the experimental conditions used. In the case of the **HNTs@Glu-OPE**, the transmittance was evaluated by subtracting the scattered light value from the nanomaterial.

The quantum yield was calculated by applying:

$$\phi_x = \left[\left(\frac{nmol_{UA_x}/s}{photons_{abs_x}/s}\eta^2\right) \Big/ \left(\frac{nmol_{UA_r}/s}{photons_{abs_r}/s}\eta^2\right)\right]\phi_r$$

where:

$$photons_{abs_x}/s = photon\ flux\ (1 - T_x)$$

$$photons_{abs_r}/s = photon\ flux\ (1 - T_r)$$

η = *solvent refractive index*

3.4. Loading of vancomycin molecules on HNTs nanomaterial

To a dispersion of **HNTs@Glu-OPE** (100 mg) in acetone (5 mL), a solution of vancomycin in H_2O (1 $0{\cdot}10^{-2}$ M, 1 mL) was added. The obtained dispersion was left stirring for 18 h at room temperature. After this time, the solvent was filtered off and the obtained powder was washed several times with acetone and left to dry at 60 °C. Loading was determined as follows. ca. 10 mg of nanomaterial were carefully weighed and washed with four portions of water (5 mL each) and the resulting solution was analyzed by UV–*vis* spectroscopy at the wavelength of 278 nm. The loading percent (LD%) and entrapment efficiency (EE%) were calculated by the following equation:

$$\mathrm{LD\%} = \frac{\mathrm{Van_{HNTs@Glu-OPE}}}{\mathrm{m_{HNTs@Glu-OPE}} + \mathrm{Van_{HNTs@Glu-OPE}}} \times 100 \quad (1)$$

$$EE\% = \frac{\mathrm{Van_{HNTs@Glu-OPE}}}{Van_{Tot}} \times 100 \quad (2)$$

where $\mathrm{Van_{HNTs@Glu\text{-}OPE}}$ and $\mathrm{Van_{Tot}}$ are the amount of vancomycin loaded on the **HNTs@Glu-OPE** nanomaterial and the total feed vancomycin, respectively, and $\mathrm{m_{HNTs@Glu\text{-}OPE}}$ is the amount of nanomaterial.

3.5. Kinetic release

The release of vancomycin molecules from **HNTs@Glu-OPE** nanomaterial was done as follows: ca. 10 mg of the sample were dispersed in 1 mL of deionized water and transferred into a sealed dialysis membrane (Medicell International Ltd MWCO 12–14,000 with a diameter of 21.5 mm). Subsequently the membrane was put in a round bottom flask containing 9 mL of the release medium (phosphate buffer (50 mM) pH 7.4 and 5.5) at 37 °C and stirred. At fixed time, 1 mL of the release medium has been withdrawn and analyzed by UV–*vis* spectroscopy at λ of 278 nm. To ensure sink conditions, 1 mL of fresh solution has been used to replace the collected one. Total amounts of drug released (F_t) were calculated as follows:

$$F_t = V_m C_t + \sum_{i=0}^{t-1} V_a C_i \quad (3)$$

where V_m and C_t are the volume and the concentration of vancomycin molecules at time *t*. V_a is the volume of the sample withdrawn and C_i is the vancomycin molecules concentration at time *i* ($i < t$).

Kinetic data were analyzed by the following mathematical model:

$$\text{Power Fit } F_t = kt^n \quad (4)$$

where F_t is the amount of vancomycin released at time *t; k* is the release constant, and *n* is the release exponent, depending on the release mechanism and the geometry of the device.

4. Conclusions

Inspired by the properties of symmetrically diglucosyl-substituted OPEs [[30] we have developed a novel divergent synthetic strategy to construct the phenyl-triple bond-ended OPE **15** (see SI). Further functionalization of the skeleton via Huisgen cycloaddition led to **Glu-OPE**, which maintains the physical and photophysical characteristics of the precursors while incorporating a suitable linker for HNTs anchoring. To the best of our knowledge, this is the first time OPE chains have been connected to halloysite nanomaterial. The dissymmetrically substituted Glu-OPE was synthesized using a copper-free Heck-Cassar-Sonogashira reaction [42], with various Pd catalysts and substrate/catalyst ratios to optimize the assembly of the molecular components. The successful linkage to the external surface of HNTs resulted in the synthesis of **HNTs@Glu-OPE**, a novel luminescent nanomaterial with promising potential as a PS. Preliminary photophysical studies with uric acid in the presence of **HNTs@Glu-OPE** demonstrated that the nanomaterial produced ROS under laser irradiation with Φ_{ROS} of 0.23, higher than that of **15**, indicating that the combination with HNTs improves the nanomaterial properties. The glucosyl moiety of **Glu-OPE**, present on the HNTs surface, promises to facilitate accumulation in cells, such as bacterial ones where the plasma membrane is rich in glycopeptides and glycolipids. Further functionalization with more complex saccharide moieties can represent a future goal for targeting such nanomaterials. Loading with vancomycin and drug kinetic release studies underscored the potential of **HNTs@Glu-OPE** as potential photosensitizer in bacterial infections. The simultaneous use of vancomycin and PDT can enhance the action against Gram-positive bacteria, such as Enterococcus, which are often multi-resistant to standard chemotherapy, and pave the way for further exploration of glycolysis-based nanosystems in advanced bacterial phototherapies.

Funding

This research did not receive any specific grant from funding agencies in the public, commercial, or not-for-profit sectors.

CRediT authorship contribution statement

Aurora Mancuso: Investigation. **Marina Massaro:** Writing – review & editing, Writing – original draft, Methodology, Formal analysis. **Federica Leone:** Writing – original draft, Investigation, Formal analysis. **Paola Maria Bonaccorsi:** Writing – review & editing, Writing – original draft. **Giuseppe Compagnini:** Methodology, Formal analysis. **Chiara Maria Antonietta Gangemi:** Methodology, Investigation. **Fausto Puntoriero:** Methodology, Investigation, Formal analysis. **Maria Ribagorda:** Investigation, Conceptualization. **Vittorio Scardaci:** Methodology, Investigation, Formal analysis. **César Viseras:** Formal analysis. **Serena Riela:** Writing – review & editing, Writing – original draft, Supervision, Investigation, Formal analysis, Conceptualization. **Anna Barattucci:** Writing – review & editing, Writing – original draft, Supervision, Investigation, Formal analysis, Conceptualization.

Declaration of competing interest

The authors declare that they have no known competing financial interests or personal relationships that could have appeared to influence the work reported in this paper.

Acknowledgements

The authors thank the University of Messina for financial support (FFABR). The publication was created with the co-financing of the European Union-FSE-REACT-EU, PON Research and Innovation 2014–2020 DM.1062/2021. F.L. is gratefully to Avviso 01/2022 – Borse regionali di ricerca in Sicilia A.A 2022/2023 – CUP: G71I22001190006 for funding her PhD scholarship. This work was supported by National Recovery and Resilience Plan (NRRP), funded by the European Union–Next Generation EU-DD 1409 Progetti di Rilevante Interesse Nazionale (PRIN) 2022 PNRR published on 14-09-2022 by the italian MUR, Missione 4 (Istruzione e Ricerca) Component 2, Investment 1.1. Project Title: Small Molecule Anticancer Ligands Library from mediterranean plants (SMALL) – CUPB53D23025910001 – Code P2022YJZ5F. Authors are also thankful for the support offered by the Spanish Project PID2022-137603013-100 (Ministerio de Ciencia, Innovación y Universidades).

Supplementary materials

Supplementary material associated with this article can be found, in the online version, at doi:10.1016/j.surfin.2025.106207.

Data availability

Data will be made available on request.

References

[1] N. Vasan, J. Baselga, DM. Hyman, A view on drug resistance in cancer, Nature 575 (2019) 299–309.
[2] M. Gopikrishnan, S. Haryini, C. GPD, Emerging strategies and therapeutic innovations for combating drug resistance in Staphylococcus aureus strains: a comprehensive review, J. Basic Microbiol. 64 (2024) 2300579.
[3] X. Hu, H. Zhang, Y. Wang, B-C Shiu, J-H Lin, S. Zhang, et al., Synergistic antibacterial strategy based on photodynamic therapy: progress and perspectives, Chem. Eng. J. 450 (2022) 138129.
[4] L. Zou, H. Wang, B. He, L. Zeng, T. Tan, H. Cao, et al., Current approaches of photothermal therapy in treating cancer metastasis with nanotherapeutics, Theranostics 6 (2016) 762–772.
[5] X. Xiong, J. Liu, L. Wu, S. Xiong, W. Jiang, P. Wang, Self-assembly strategies of organic small-molecule photosensitizers for photodynamic therapy, Coord. Chem. Rev. 510 (2024) 215863.
[6] S. Lee, S. Min, G. Kim, S. Lee, Recent advances in the design of organic photothermal agents for cancer treatment: a review, Coord. Chem. Rev. 506 (2024) 215719.
[7] W. Zhang, A. Ahmed, H. Cong, S. Wang, Y. Shen, B. Yu, Application of multifunctional BODIPY in photodynamic therapy, Dyes Pigments 185 (2021) 108937.
[8] S. Monro, K.L. Colón, H. Yin, J. Roque III, P. Konda, S. Gujar, et al., Transition metal complexes and photodynamic therapy from a tumor-centered approach: challenges, opportunities, and highlights from the development of TLD1433, Chem. Rev. 119 (2019) 797–828.
[9] S. Mehrzad Sajjadinezhad, L. Boivin, K. Bouarab, P.D. Harvey, Photophysical properties and photonic applications of porphyrin-based MOFs, Coord. Chem. Rev. 510 (2024) 215794.
[10] X. Chen, J. Li, S. Roy, Z. Ullah, J. Gu, H. Huang, et al., Development of polymethine dyes for NIR-II fluorescence imaging and therapy, Adv. Healthc. Mater. 13 (2024) 2304506.
[11] L. Lv, B. Fan, X. Ji, Y. Liu, T. Chen, Y. Li, et al., From the clinical perspective of photodynamic therapy and photothermal therapy: structure-activity-practice, Coord. Chem. Rev. 507 (2024) 215733.
[12] R. Yan, M. Zhan, J. Xu, Q. Peng, Functional nanomaterials as photosensitizers or delivery systems for antibacterial photodynamic therapy, Biomater. Adv. 159 (2024) 213820.
[13] B. Sun, H. Chen, Y. Wang, X. Wang, W.H.Z. He, C. Xie, et al., Development of mesoporous silica-based nanoparticles for cancer phototherapy, Dyes Pigments 222 (2024) 111881.
[14] T.P. Premji, B.S. Dash, S. Das, J-P. Chen, Functionalized nanomaterials for inhibiting ATP-dependent heat shock proteins in cancer photothermal/ photodynamic therapy and combination therapy, Nanomaterials 14 (2024) 112.
[15] M. Massaro, R. Ciani, G. Cinà, C.G. Colletti, F. Leone, S. Riela, Antimicrobial nanomaterials based on halloysite clay mineral: research advances and outlook, Antibiotics 11 (2022) 1761.
[16] N. Gray-Wannell, P. Cubillas, Z. Aslam, P.J. Holliman, H.C. Greenwell, R. Brydson, et al., Morphological features of halloysite nanotubes as revealed by various microscopies, Clay. Miner. 58 (2023) 395–407.
[17] O. Prinz Setter, E. Segal, Halloysite nanotubes – the nano-bio interface, Nanoscale 12 (2020) 23444–23460.
[18] S. Riela, A. Barattucci, D. Barreca, S. Campagna, G. Cavallaro, G. Lazzara, et al., Boosting the properties of a fluorescent dye by encapsulation into halloysite nanotubes, Dyes Pigments 187 (2021) 109094.
[19] S. Riela, A. Borrego-Sánchez, S. Cauteruccio, R. de Melo Barbosa, M. Massaro, C. I. Sainz-Díaz, et al., Exploiting the interaction between halloysite and charged PNAs for their controlled release, J. Mater. Chem. B 11 (2023) 6685–6696.
[20] A.P. Falanga, M. Massaro, N. Borbone, M. Notarbartolo, G. Piccialli, L.F. Liotta, et al., Carrier capability of halloysite nanotubes for the intracellular delivery of antisense PNA targeting mRNA of neuroglobin gene, J. Colloid. Interface Sci. 663 (2024) 9–20.
[21] M. Massaro, G. Ghersi, R. de Melo Barbosa, S. Campora, S. Rigogliuso, R. Sànchez-Espejo, et al., Nanoformulations based on collagenases loaded into halloysite/ Veegum® clay minerals for potential pharmaceutical applications, Colloids Surf. B Biointerfaces 230 (2023) 113511.
[22] M. Massaro, M. Laura Alfieri, G. Rizzo, F. Babudri, R. Barbosa de Melo, T. Faddetta, et al., Modification of halloysite lumen with dopamine derivatives as filler for antibiofilm coating, J. Colloid. Interface Sci. 646 (2023) 910–921.
[23] M. Massaro, A. Borrego-Sánchez, R. Sánchez-Espejo, C. Viseras Iborra, G. Cavallaro, F. García-Villén, et al., Ciprofloxacin carrier systems based on hectorite/halloysite hybrid hydrogels for potential wound healing applications, Appl. Clay. Sci. 215 (2021) 106310.
[24] Z. Fernández, L. Sánchez, S. Santhosh Babu, G. Fernández, Oligo (phenyleneethynylene)s: shape-tunable building blocks for supramolecular self-assembly, Angew. Chem. Int. Ed. 63 (2024) e202402259.
[25] P-H Lanoë, T. Gallavardin, A. Dupin, O. Maury, P.L. Baldeck, M. Lindgren, et al., Influence of bromine substitution pattern on the singlet oxygen generation efficiency of two-photon absorbing chromophores, Org. Biomol. Chem. 10 (2012) 6275–6278.
[26] D. Dascier, E. Ji, A. Parthasarathy, K.S. Schanze, D.G. Whitten, Efficacy of end-only-functionalized oligo(arylene-ethynylene)s in killing bacterial biofilms, Langmuir 28 (2012) 11286–11290.
[27] W. Liao, L.-g. Zhuo, X. Yang, P. Zhao, W. Kan, G. Wang, et al., Biocidal activity and mechanism study of unsymmetrical oligo-phenylene-ethynylenes, ACS. Appl. Bio Mater. 3 (2020) 5644–5651.
[28] A.M. Fanni, D. Okoye, F.A. Monge, J. Hammond, F. Maghsoodi, T.D. Martin, et al., Controlled and selective photo-oxidation of amyloid-β fibrils by oligomeric p-phenylene ethynylenes, ACS Appl. Mater. Interfaces 14 (2022) 14871–14886.
[29] A. Barattucci, E. Deni, P. Bonaccorsi, M.G. Ceraolo, T. Papalia, A. Santoro, et al., Oligo(phenylene ethynylene) glucosides: modulation of cellular uptake capacity preserving light ON, J. Org. Chem. 79 (2014) 5113–5120.
[30] E. Deni, A. Zamarrón, P. Bonaccorsi, M. Carmen Carreño, Á Juarranz, F. Puntoriero, et al., Glucose-functionalized amino-OPEs as biocompatible photosensitizers in PDT, Eur. J. Med. Chem. 111 (2016) 58–71.
[31] A. Lara-Pardo, A. Mancuso, S. Simón-Fuente, P.M. Bonaccorsi, C.M.A. Gangemi, MÁ Moliné, et al., Amino-OPE glycosides and blue light: a powerful synergy in photodynamic therapy, Org. Biomol. Chem. 21 (2023) 386–396.
[32] C. Geng, S. Pang, R. Ye, J. Shi, Q. Yang, C. Chen, et al., Glycolysis-based drug delivery nanosystems for therapeutic use in tumors and applications, Biomed. Pharmacother. 165 (2023) 115009.
[33] G.B. Giovenzana, L. Lay, D. Monti, G. Palmisano, L. Panza, Synthesis of carboranyl derivatives of alkynyl glycosides as potential BNCT agents, Tetrahedron 55 (1999) 14123–14136.
[34] C. Yi, C. Blum, M. Lehmann, S. Keller, S-X Liu, G. Frei, et al., Versatile strategy to access fully functionalized benzodifurans: redox-active chromophores for the construction of extended π-conjugated materials, J. Org. Chem. 75 (2010) 3350–3357.
[35] D. Chan-Seng, J-F. Lutz, Primary structure control of oligomers based on natural and synthetic building blocks, ACS Macro Lett. 3 (2014) 291–294.
[36] M. Massaro, P. Poma, G. Cavallaro, F. García-Villén, G. Lazzara, M. Notarbartolo, et al., Prodrug based on halloysite delivery systems to improve the antitumor ability of methotrexate in leukemia cell lines, Colloids Surf. B Biointerfaces 213 (2022) 112385.
[37] M. Casiello, S. Savino, M. Massaro, L.F. Liotta, G. Nicotra, C. Pastore, et al., Multifunctional halloysite and hectorite catalysts for effective transformation of biomass to biodiesel, Appl. Clay. Sci. 242 (2023) 107048.
[38] B.R. Rabello, A.P. Gerola, D.S. Pellosi, A.L. Tessaro, J.L. Aparício, W. Caetano, et al., Singlet oxygen dosimetry using uric acid as a chemical probe: systematic evaluation, J. Photochem. Photobiol. A Chem. 238 (2012) 53–62.
[39] A. Di Poto, M.S. Sbarra, G. Provenza, L. Visai, P. Speziale, The effect of photodynamic treatment combined with antibiotic action or host defence mechanisms on Staphylococcus aureus biofilms, Biomaterials 30 (2009) 3158–3166.
[40] M. Massaro, F. Armetta, G. Cavallaro, D.F. Chillura Martino, M. Gruttadauria, G. Lazzara, et al., Effect of halloysite nanotubes filler on polydopamine properties, J. Colloid. Interface Sci. 555 (2019) 394–402.
[41] P.D. Cotter, C. Hill, Surviving the acid test: responses of gram-positive bacteria to low pH, Microbiol. Mol. Biol. Rev. 67 (2003) 429–453.
[42] R. Chinchilla, C. Nájera, The Sonogashira reaction: a booming methodology in synthetic organic chemistry, Chem. Rev. 107 (2007) 874–922.